Journal Pre-proof

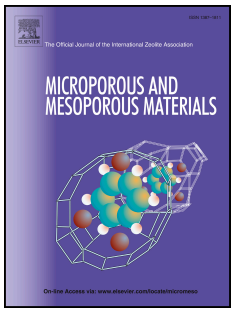

Identification of an efficient adsorbent for ethanol sensing at room temperature using quartz crystal microbalance

Mohit Kumar, Achraf EL. Mohajir, Franck Berger, Marina Raschetti, Jean-Baptiste Sanchez

PII: S1387-1811(22)00187-1

DOI: https://doi.org/10.1016/j.micromeso.2022.111869

Reference: MICMAT 111869

To appear in: *Microporous and Mesoporous Materials*

Received Date: 24 January 2022

Revised Date: 16 March 2022

Accepted Date: 26 March 2022

Please cite this article as: M. Kumar, A.E. Mohajir, F. Berger, M. Raschetti, J.-B. Sanchez, Identification of an efficient adsorbent for ethanol sensing at room temperature using quartz crystal microbalance, *Microporous and Mesoporous Materials* (2022), doi: https://doi.org/10.1016/j.micromeso.2022.111869.

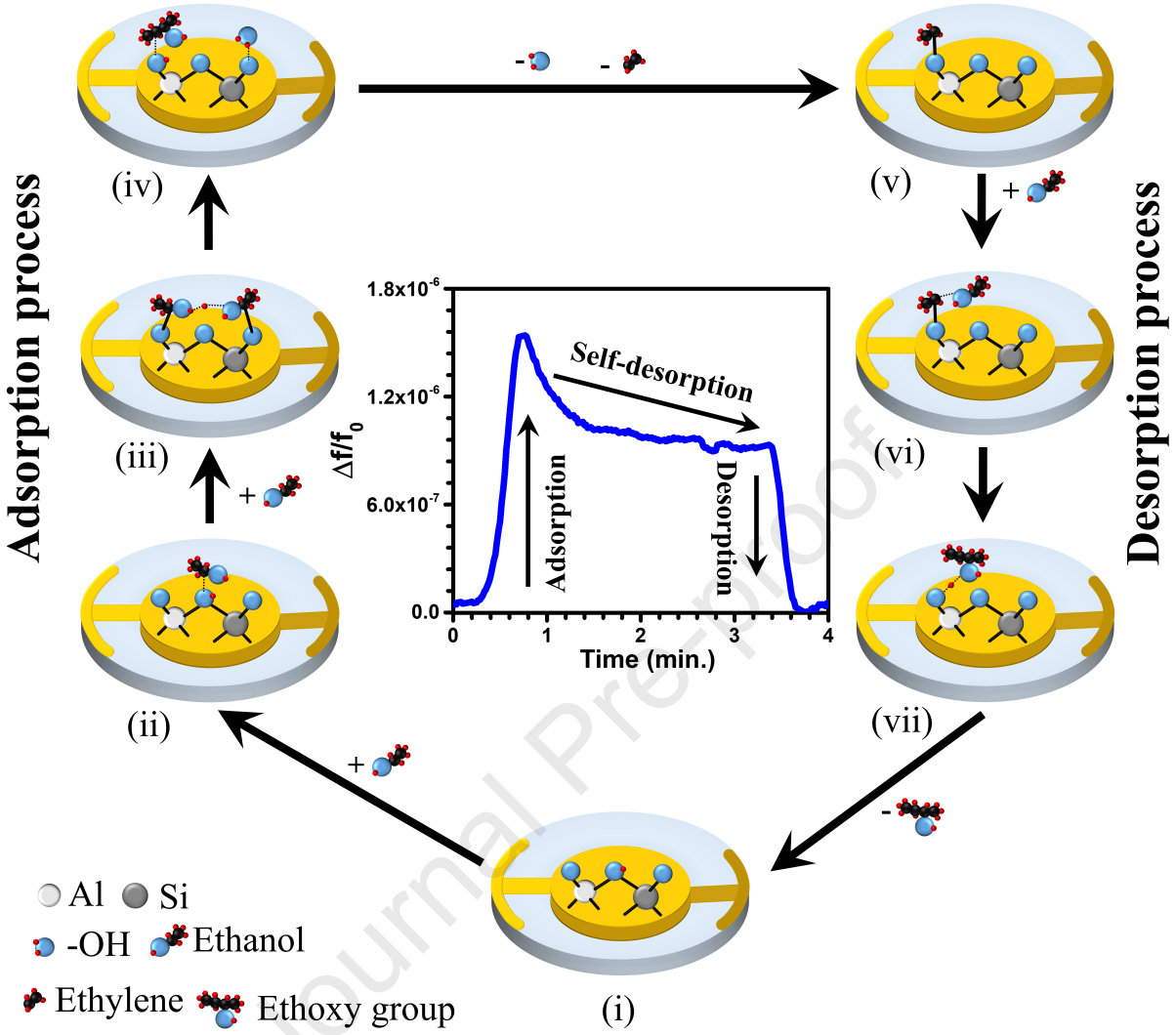

Identification of an efficient adsorbent for ethanol sensing at room temperature using quartz crystal microbalance

Mohit Kumar[a*], Achraf EL Mohajir[a], Franck Berger[a], Marina Raschetti[a], and Jean-Baptiste Sanchez[a]

[a]Institut FEMTO-ST, UMR CNRS 6174, Université Bourgogne Franche-Comté, 15B Avenue des montboucons, 25030 Besançon, France

*Corresponding author: e-mail: mohit.kumar@femto-st.fr

Abstract

Zeolite coated quartz crystal microbalance (QCM) is proposed as an efficient sensor for the detection of ethanol at room temperature. In this work, three zeolites DaY, ZSM-5, and BEA were investigated in order to determine the most efficient adsorbent for ethanol sensing at room temperature. The sensing performances were found to be mostly influenced by the acid site density and the zeolite's pore size. The BEA coated QCM sensor exhibited the best performances with a high relative frequency shift from 9.0×10^{-7} to 2×10^{-6} for 10 ppm of ethanol. Furthermore, this sensor exhibited fast response and recovery times which makes it a suitable material for the monitoring of ethanol in the air. In addition, the ethanol diffusion order was evaluated using Fickian diffusion law and was found to be the highest for the zeolite BEA. A sensing mechanism was also proposed for the adsorption and desorption of ethanol into zeolites based on unstable protonated dimers, water and diethyle ether resides for the energy-efficient ethanol sensor.

Keywords: Zeolites; Brønsted and Lewis acid sites; Adsorption-desorption; Adsorbent coated QCM sensor; Relative frequency shift.

1. Introduction

Air quality is a crucial determinant of a healthy life and people's well-being, consequently air quality has attracted a lot of attention in recent years with the increasing levels of toxic chemicals found in the air. The health effects of these toxic chemicals vary greatly, from eye, nose, and throat irritation, to damage to the liver, kidney, or central nervous system, and in some cases even premature deaths [1–3]. Therefore, the development of highly sensitive sensors with fast response and low power consumption is of the utmost importance for the continuous monitoring of these compounds. Ethanol, listed as a toxic chemical, is widely used in the food, medical, cosmetic, oil refineries, and alcoholic beverage industries [4–6]. This compound is considered to be a hypnotic chemical that can cause several health issues such as the irritation of the eyes, difficulty in breathing, headache, drowsiness, and in some cases even cancer [2,4,7]. Moreover, the presence of ethanol in closed spaces is considered to be a fire hazard due to its highly flammable nature. This brings the need for systems capable of detecting ethanol at low concentrations (few ppm) without any external heating source (at room temperature). In the last few years, owing to their size-selective porosity and efficient chemical catalytic properties at room temperature [8–11], zeolites have seen their use for gas sensing applications. The choice of the most suitable zeolite is based on many characteristics such as the pore size, channel dimensions, catalytic behaviors, and especially Brønsted and Lewis acid sites density [12–16]. Their structure is formed by $(SiO_4)^{4-}$ and $(AlO_4)^{5-}$ tetrahedral (T) that share oxygen atoms to form a T-O-T with an angle between 130° and 180°. Tetrahedral are capable of combining in a variety of framework structures of limited aperture size over membered rings (MR) channels [17–19]. The acid sites in the zeolites are cropped up by the coordination of Al atoms in the framework under the necessity of charge-compensation to yield a neutral material. The presence of acid sites can have a major influence on the selective adsorption of gas molecules in zeolites [20,21]. Brønsted and Lewis are the two types of acid

sites found in zeolites. Brønsted acid site is "a molecular entity capable of donating a hydrogen (proton) to a base or corresponding chemical species". On the other hand, the Lewis acid site is "a molecular entity that can accept an electron pair from the donor compound" [22,23]. Fig. 1 shows the schematic of Brønsted and Lewis acid sites in zeolites [24].

Recently, several studies focused on zeolites to use it as a sensing material by itself or to enhance the performances of gas sensors (sensitivity, selectivity, response and recovery times) [25,26]. Among all these techniques, zeolite coated quartz crystal microbalance (QCM) based gas sensors seem to be an efficient way for the real-time monitoring of ethanol at room temperature. This technique consists of depositing or coating zeolites on a QCM to measure ethanol uptake and release. This technique is generally non-reliant on external heating and also label-free for the adsorption and the desorption phases during the physical/chemical processes of ethanol molecules on the zeolite's surface [27–29]. The resonance frequency of resonator change (Δf) is caused by the change in the mass (Δm) on the quartz crystal of QCM due to the adsorption of ethanol on the zeolite's surface according to Sauerbrey's equation [30]

$$\Delta f = -\frac{2f_0^2}{A\sqrt{\rho_q \mu_q}}\Delta m \qquad (1)$$

Where A, f_0, ρ_q and μ_q are the active area, initial frequency, density (2.648 g/cm^3) and Shear modulus (2.947×10^{11} g/cm.s^2) of the quartz crystal, respectively.

Out of the many available zeolites, the faujasite (FAU)-type zeolites are considered to be the most open framework of naturally occurring zeolites. For instance, the FAU framework of DaY consists of large sodalite cages (~11 Å) that are interconnected in a cubic manner over 12-rings channels with an aperture size of 7.4 Å [31–33]. The MFI framework of ZSM-5 has an arrangement of six secondary building units in order for 5-1 groups to combine and form a pentasil-like structure. This arrangement consists of straight channels that are interconnected by perpendicular sinusoidal channels over a 10-rings system. For ZSM-5, the straight and sinusoidal channels have an aperture of 5.4 × 5.6 and 5.1 × 5.5 Å [34,35]. On the other hand,

the beta-type zeolites have two topologically identical linear channel systems that are mutually orthogonal and perpendicular to the [001] plane in three poly-types combinations (a) 2 polymorphs, (b) polymorph A (BEA), and, (c) polymorph B (BEB) [36,37]. Zeolite BEA has a three-dimensional flexible framework due to the presence of straight channels with a diameter of 6.6 × 6.7 Å and perpendicular sinusoidal channels with a diameter of 5.6 × 5.7 Å over a 12-rings pore system [38,39]. In this work, we studied the effect of ethanol concentrations on the sensing performances of three different porous structure zeolites DaY, ZSM-5, and BEA of FAU, MFI and beta frameworks, respectively. These zeolites were selected based on their distinct frameworks, porous volume, different surface properties and pore sizes (higher than the kinetic diameter of ethanol). The textural properties of each zeolite were evaluated using N_2 adsorption-desorption isotherms. In addition, a morphological characterization was done using the SEM technique and the chemical signatures were studied using FTIR spectroscopy. The identification of an efficient zeolite for ethanol sensing at room temperature was done using a zeolite coated QCM by measuring their sensing properties at different concentrations. The order of diffusion coefficient was successfully estimated in DaY, ZSM-5, and BEA zeolites using Fickian diffusion law, and a schematic of the ethanol sensing mechanism in zeolites was proposed based on our observations.

2. Experimental Details

2.1 Adsorbents

Three zeolites were deposited on the quartz specs of QCM in order to investigate their sensing capabilities. Dealuminated (DaY) faujasite zeolite, with a chemical formula $Na_2(Al_2Si_{190}O_{384})$, was purchased from Degussa with a particle size in the range 1-5 μm. Zeolite Socony Mobil (ZSM-5) and Beta polymorph A (BEA) were obtained using hydrothermal treatment from concentrated reaction mixtures in the laboratory of Interdisciplinaire Carnot de Bourgogne,

Dijon. More details can be found in [40–42]. The Si/Al ratio in DaY, ZSM-5, and BEA is estimated to be 95, 50, and 25, respectively.

2.2 Characterizations of Adsorbents

The textural properties of zeolites were characterized by N_2 adsorption-desorption isotherms at 77 K using a Micromeritics ASAP 2020 sorptometer for DaY and Sorptomatic 1990 (Thermo Electron Corp.) for ZSM-5 and BEA. The surface area (A_{BET}) and the pore size were calculated using the BET equation and Saito-Foley method, respectively. The deposition of a uniform layer of zeolites on the quartz crystal of QCM was confirmed by using FESEM (FEI Helios Nanolab 600i) technique. The identification of functional groups and chemical signatures were obtained using FTIR (PIKE MIRacle single reflection ATR) characterization technique.

2.3 Zeolite coated QCM sensors and ethanol sensing measurements

10 mg of zeolite powder was dissolved in 5 mL of pure ethanol and the solution was stirred using a magnetic stirrer for 4 hours in a closed neck glass bottle. Following this step, the zeolites were deposited on the Au/Ti electrodes of quartz specs of QCM using an air-gun spray method. During the deposition, the air pressure was kept below 0.25 bar and a polyethylene mask with an opening of 5 mm was used for a localized deposition on the Au/Ti electrode of quartz specs to avoid unwanted spread of the adsorbent on its surface. The quartz specs were kept in ambient air at room temperature for 40 hours to allow the evaporation of the solvent. Fig. 2 (a) shows a photograph of the pristine quartz specs which is ~ 13.9 mm in diameter with its Au/Ti electrodes in the center and a photograph of the adsorbent (BEA) deposited on the quartz specs. The diameter of the deposited adsorbent layer was measured at ~ 5.0 mm and with a weight of ~ 0.1 mg. In this work, all the adsorbents were deposited with an equally active area and nearly identical weight on the quartz specs electrodes. For ethanol sensing, each

adsorbent coated quartz specs was mounted on the QCM platform (purchased from Novaetech S. r. l.) which included an oscillator circuit loop. The output frequency was set on 10 MHz using an open QCM 1.2 computational program. First, each sensor was kept under synthetic air (~ 8 % relative humidity at 25 °C) with a flow rate of 200 mL/min at room temperature for 1 hour to stabilize the QCM by achieving a constant frequency. The accuracy of the frequency measurement was estimated at ± 2 Hz. The same synthetic air was also used as a carrier gas for ethanol vapors and the dilution was done by changing the ratio between the airflow and ethanol. Ethanol concentrations were measured using the SGP30 ethanol sensor (purchased from Sensirion) with an accuracy of ± 3 ppm. The ethanol sensing measurements were performed at room temperature with concentrations of 10, 20, and 30 ppm.

3. Results and discussion

3.1 Adsorbent characterizations

Fig. 2 (b) shows the N_2 adsorption – desorption isotherms of DaY, ZSM-5, and BEA materials. High N_2 uptakes were observed at low relative pressures ($P/P_0 < 0.01$) showing the existence of narrow micropores. The adsorption – desorption hysteresis loops correspond to H4 for DaY and ZSM-5 and type IV for BEA according to the IUPAC classification. This indicates that DaY and ZSM-5 consist mainly of micropores and few mesopores while BEA is composed of micro and mesopores. The channel system and textural properties of each adsorbent are listed in Table.1 [40,42–44].

The calculated A_{BET} were 393 and 529 $m^2\ g^{-1}$ for ZSM-5 and BEA, respectively, and slightly higher for the DaY, around 716 $m^2\ g^{-1}$. However, the porosity present in DaY and ZSM-5 consists mainly of micropores that represent more than 90 % of the total pore volume, while the micropore volume of and BEA only represents 33 % of the total pore volume. The average pore diameter was estimated to be around 5.5, 7.5 and 11.2 Å for ZSM-5, BEA and DaY

respectively. The kinetic diameter for ethanol being 4.3 Å, the chosen zeolites for this study represent a viable choice to trap ethanol as the molecules can enter the pores of the selected materials.

Fig. 2 (c) shows the SEM images of DaY, ZSM-5, and BEA collected directly from the coated quartz specs of QCM. The surface of the DaY layer is composed of identical crystals with a typical grain size of hundreds of nm. Polygonal platelets were observed on the surface of the ZSM-5 layer with a grain size between 0.1 to 1.5 μm. In the case of BEA, the surface is covered with nearly identical spheroidal particles with a typical size between 70 nm and 1.3 μm.

Fig. 3 shows the FTIR spectra of DaY, ZSM-5 and BEA zeolites obtained in the range of 1300 to 4000 cm^{-1}. Each spectrum was recorded with a 4 cm^{-1} spectral resolution. The main feature of the DaY spectrum is the presence of bands at 1410 and 1590 cm^{-1} that correspond to Lewis acid (LA) and Brønsted acid (BA) sites [45,46], respectively. The BA band is more intense compared to LA band, which may indicate a more significant active participation of BA sites in the DaY framework. A broad band is detected at 3410 cm^{-1} with a shoulder at 3690 cm^{-1} in the high frequency range that corresponds to OH stretching in Si-OH and Si-OH-Al groups. Similar low intensity LA and BA bands are detected in pristine ZSM-5. These bands are observed at higher frequencies (1450 and 1660 cm^{-1}, respectively), and are shifted compared to the DaY. This shift could be due to the different structure, chemical composition and stoichiometry. The OH stretching broad band for ZSM-5 is also detected in the high frequency range at 3450 cm^{-1}. The main feature of the BEA spectrum is that the intense LA band is detected at 1410 cm^{-1} , with this band corresponding to bridging extra-framework aluminium species [20,21]. Low intensity BA band is also detected at 1600 cm^{-1} and OH stretching broad band at 3410 cm^{-1}.

The presence of strong LA and BA sites and OH stretching bands in the FTIR spectrum of adsorbents are attributed to the chemisorption along with the physisorption. The chemisorption can occur owing to the ethanol dehydration over the zeolites. As reported in the literature, an ethanol molecule is adsorbed at a proton site to form a hydrogen-bonded ethanol monomer and form unstable dimeric species following another ethanol's molecule adsorption (schematized in Fig. 4 (a) and (b)). In the dimeric intermediate, the proton is placed between alcohol and oxygen atoms and subsequently, the protonated dimers are rearranged and decomposed into water causing an adsorbed diethyl ether that desorbs to regenerate the proton site (see Fig. 4 (c)). The occurrence of protonated ethanol dimers through ethanol dehydration on zeolitic catalysts was confirmed in previous reports [47–49].

Another point is that the presence of silanol groups, anionic charges, and cations in the external surface of zeolites help the formation of local electrostatic fields that can contribute to the adsorption of ethanol. [50–52]. The presence of the intense LA band which corresponds to the bridging of extra-framework aluminum species in BEA zeolite can allow the volumetric adsorption of ethanol by the formation of alcohol-water dimer, alcohol-water-hydronium ion clusters, or extended hydrogen-bonded water network [53].

3.2 Ethanol sensing characterizations

A study under a controlled environment was performed using the adsorbent coated quartz specs QCM to evaluate the effect of the porous structures on ethanol sensing. The performance of the resonator sensor was evaluated with ethanol adsorption and desorption processes at room temperature for different concentrations. The sensor's performances can also be evaluated based on its specific characteristics such as the relative response, response time, recovery time, and repeatability. Fig. 5 shows the sensor's relative frequency ($\Delta f/f_0$) curves as a function of

time after a baseline correction, for (a) DaY, (c) ZSM-5, and (e) BEA coated QCM sensors with different ethanol concentrations (10, 20, and 30 ppm). The sensor's response time (t_{Rs}) and recovery time (t_{Rv}) are the recorded time to reach 90% of the saturation point and the time required to return to 90% of the initial frequency, respectively [54]. The corresponding t_{Rs} and t_{Rv} change with ethanol concentration are summarized for each zeolite in Fig. 5 (b), (d), and (f).

Two out of five measured curves are presented for each concentration, all the recorded curves were found to be similar which shows a good repeatability of the sensor for ethanol detection. The error-bars were calculated as the standard deviation from 5 trials. It was observed that the relative frequency increases with ethanol adsorption and reaches a saturation point followed by a decrease caused by the desorption of ethanol molecules returning to its initial baseline. These results show that the zeolite coated QCM sensors exhibited a good repeatability as well as a good reversibility.

Fig. 5 (a) and (b) show the ethanol transients, response, and recovery times for DaY. The main feature of the DaY is that the saturation point was achieved rapidly (28 s) at 1.4×10^{-7} with a low relative frequency shift. Similarly, the desorption process was also completed very quickly with 10 ppm of ethanol (72 s). No significant changes were observed with higher concentrations of ethanol, the main difference is observed in the value of the saturation point which was found to be slightly lower at 1.2×10^{-7} for 30 ppm. The saturation point and the adsorption-desorption curves are not affected significantly with an increasing ethanol concentration revealing that the cage of DaY is filled rapidly. This can be explained by the fact that most of the porosity present in DaY is microporous which limits the accessibility to the entire porous space. Another important characteristic of the gas sensor is the sensing kinetic. The response time decreases linearly with increasing ethanol concentrations from 0.47 ± 0.15

to 0.20 ± 0.04 min. for DaY. Essentially, during the adsorption, this might be due to additional ethanol molecules that are being trapped at available surface sites with the increasing concentration and will occupy space in the adsorbent's geometry faster compared to low concentrations. Moreover, the drop observed for t_{Rv} could be a result of the presence of large pores (11.2 Å) that allow an easy exit of ethanol molecules. In the case of ZSM-5, the saturation point was achieved very slowly at 2.3×10^{-6} relative frequency for 10 ppm of ethanol (see Fig. 5 (c)). The different ethanol concentrations seem to not influence the sensing performances of ZSM-5 coated QCM. This could be due to the involvement of a secondary internal network accessed by ethanol in the MFI framework [56–58] that can enhance the deeper diffusion of ethanol molecules in the framework and gradual adsorption characteristics. The drop in the relative frequency shift with increasing ethanol concentrations may be due to the presence of water or ether resides and low density of Brønsted acid sites in ZSM-5 [22, 60]. N. Pfriem *et al*. [55] have studied the role of the ionic environment in enhancing the activities of reacting molecules in zeolite's pores and found that the adsorption rate drops at higher concentrations of reacting molecules, due to the residing nature of protonated dimers and water in the zeolite's micropore channels. This phenomenon can cause the space between two protonated boundaries to be changed equivalently as available electrolytes and the adsorption of reacting molecules can also be affected by the Brønsted acid sites density in MFI. Fig. 5 (d) shows the response and recovery times for ZSM-5. The t_{Rs} and t_{Rv} values support the idea of water or ether residing inside the structure as explained above, as they remain practically unchanged regardless of the ethanol concentration with an average value of 6.32 ± 0.38 min. and 6.26 ± 0.23 min. for the response time and recovery time, respectively. The dynamic responses of ethanol sensing for BEA are presented in Fig. 5 (e). The main attribute of BEA is that the saturation point was achieved rapidly at 9×10^{-7} with a high relative frequency. This shows that BEA exhibits a high affinity towards ethanol and allows an easy access to the mesopores [39,56]. A slight drop

of the relative frequency was observed after the saturation point was reached which can be explained by the self-desorption character of adsorbed ethanol. The well-connected porosity in BEA is in full display as the response increases with increasing ethanol concentrations. The rise in relative frequency with ethanol concentration can also be attributed to the presence of a high density of Lewis acid sites as observed in the FTIR spectrum for BEA. The local environment of Lewis acid sites creates the extra-framework metal or Al active species in three-coordination and forms adjacent silanol groups that support more ethanol adsorption [57]. Thus, the high-density of Lewis acid sites supports the ethanol adsorption with a high concentration in BEA. Fig. 5 (f) shows the response and recovery times for BEA that were found similar to those observed for DaY. The response time decreases linearly with increasing ethanol concentrations from 0.63 ± 0.12 to 0.3 ± 0.06 min. due to the slow diffusion inside the porous network of BEA. A similar behavior was observed for the recovery time decreasing from 0.3 ± 0.03 to 0.2 ± 0.04 min. for 10 to 20 ppm and does not change significantly for 30 ppm. This shows that ethanol molecules are following a similar desorption pathway up to a certain point and leave occupied space that might be disrupted by residing molecules. Table 2 shows the comparison between this work and reported previous methods based on the sensor response, response time, and recovery time at room temperature for ethanol detection.

Compared to other room temperature operated ethanol sensors, we found that the BEA coated QCM sensor shows a high sensor response for ethanol in low concentrations (few ppm). The response and recovery times were also shorter than other sensors in the same range of ethanol concentrations (around 10 ppm). This proves that the use of zeolite coated QCM sensors represents an easy method for the rapid detection of ethanol in air.

Zeolite based gas sensor properties depend also on the diffusion behavior of gas molecules into its framework. The order of the diffusion coefficient of ethanol was estimated for DaY, ZSM-

5 and BEA by applying Fickian diffusion law. We assume a constant diffusivity that is independent of local ethanol concentrations. Using Fickian diffusion law, the mass uptake during diffusion is predicted as [58]:

$$\frac{M_f(t)}{M_\infty} = 1 - \frac{8}{\pi^2}\sum_{n=0}^{\infty}\frac{1}{(2n+1)^2}\exp\left(-\frac{4D\,(2n+1)^2\,\pi^2 t}{L^2}\right) \qquad (2)$$

Where M_∞ is the mass loading at saturation, $M_f(t)$ is the mass loading in t time, L is the adsorbent film thickness and D is the diffusion coefficient. When $\frac{M_f(t)}{M_\infty}$ is plotted *vs.* $t^{1/2}$, this curve produces a linear part for the initial stage of the adsorption phase. The slope of this linear part provides the diffusion coefficient. More specifically, the frequency of the QCM sensor is shifted with the mass loading of ethanol, one has:

$$\frac{M_f(t)}{M_\infty}\ or\ \frac{f_t}{f_\infty} \approx \frac{8}{\sqrt{\pi}}\sqrt{\frac{Dt}{L^2}} \qquad (3)$$

The slop from plot $\frac{f_t}{f_\infty}$ vs. $t^{1/2}$ curves can give an estimation of the order of ethanol diffusion coefficient for DaY, ZSM-5, and BEA. Fig. 6 shows the plot of $\frac{f_t}{f_\infty}$ vs. $t^{1/2}$ for (a) DaY, (b) ZSM-5, and (c) BEA with the initial point linear fitting for each one in red. We found that the slope is changing in order of DaY (0.059 ± 0.024) < ZSM-5 (0.101 ± 0.012) < BEA (0.249 ± 0.026). This reveals that the ethanol diffusion into BEA (Beta frameworks) is more favorable compared to other adsorbents. This means that the BEA represents a suitable zeolite for ethanol sensing applications. Furthermore, the total acid site density that affects the extra-framework available aluminum species in each adsorbent is different in DaY, BEA, and ZSM-5. These species are responsible for the neutralization of Brønsted acid sites, blocking access to Brønsted acid sites, or enhancing ethanol interactions with the surface by the formation of super Lewis acid sites that are more favorable to ethanol's molecules adsorption [59]. To sum up, on top of the mesopore volume in BEA, the presence of extra-framework aluminum species enhances the ethanol sensing properties.

4. Sensing mechanism

The mass sensitive zeolite coated QCM sensor mechanism depends on the interactions between the adsorbent's surface and ethanol molecules during the adsorption for the mass increase and during the desorption for mass decrease on QCM. This interaction can take place through physisorption or chemisorption process or both. Based on experimental investigation, an ethanol sensing mechanism is proposed and schematized in Fig. 7, where steps (i) to (iv) are devoted to the adsorption process and steps (v) to (vii) including (i) are devoted to the desorption process of ethanol. The sensing mechanism is mainly governed by weak O···C-H and typical O-H···O bonds on the zeolite's surface and the change in mass on the quartz specs that are responsible for the frequency shift of the zeolite coated QCM sensor. In the adsorption process, step (i) when the zeolite coated QCM is loaded with ethanol, an ethanol molecule is adsorbed at the proton sites to form O···C-H bonded ethanol monomer, see step (ii). By the adsorption of another ethanol molecule in close proximity (the nearest neighbor), the dimer species are formed, as shown in step (iii). In the intermediate of the dimer, the proton can be held between the alcohol and oxygen atoms. These protonated dimers are capable of rearranging and decomposing inwater and an adsorbed diethyl ether (Ethoxy group), step (iv). The formation of protonated ethanol dimers was confirmed in previous studies during ethanol dehydration on zeolite catalysts [48,60,61]. The ethoxy group can transform whereas acid sites are regenerated and as a result can provide ethylene [62,63]. The desorption process begins with the elimination of water and ethylene from the zeolite's surface, step (v). Similar to step (ii), the presence of another ethanol molecule on the zeolite's surface is capable of forming ethanol monomer and this intermediate is transformed to an ethoxy group by replacing the proton in the Si (O^-) Al sites and is also able to form an ethanol-ethoxy pair on adjacent oxygen, step (vi). Ethanol-ethoxy pair forms diethyle ether, step (vii) which is desorbed by regenerating

the acid sites which induces a mass decrease on the zeolite coated quartz specs of QCM, and the sensor start to resonate at its initial frequency.

5. Conclusions

In this study, we investigated the ethanol sensing performances of three different zeolites (DaY, ZSM-5, and BEA) coated QCM sensors at room temperature. The mesoporous network of the aforementioned zeolites is a key parameter in the detection of ethanol which allows the access of molecules to the microporosity. The mesoporous volume was estimated to be 7 %, 10 %, and 67 % for the DaY, ZSM-5, and BEA, respectively. Additionally, the high Lewis acid sites density in BEA confirmed by FTIR results tends to favor ethanol volumetric adsorption in comparison to the other zeolites. In the case of the BEA coated QCM, the compensating cations played a major role in the adsorption and desorption of ethanol resulting in good sensing performances with the highest response (relative frequency shift in the order of 2×10^{-6}), the fastest response time (~ 38 s) and recovery time (~ 18 s) for 10 ppm of ethanol. The ethanol sensing mechanism in the zeolite-based sensor was also proposed which is mainly attributed to the chemisorption of ethanol supported by the formation of the unstable protonated dimers and water and diethyl ether resides. Therefore, the proposed BEA coated QCM sensor showed good sensing performances while operating at room temperature which makes it a suitable energy-efficient sensor for the rapid detection of ethanol.

Acknowledgments

The authors would like to express their gratitude to the Bourgogne Franche-Comté Region, the European fund FEDER, and the EUR EIPHI for financial support through the project DECOLAIR. This work was partially supported by the French RENATECH network and its FEMTO-ST technological facility.

References

[1] D.W. Lachenmeier, Safety evaluation of topical applications of ethanol on the skin and inside the oral cavity, J. Occup. Med. Toxicol. Lond. Engl. 3 (2008) 26. https://doi.org/10.1186/1745-6673-3-26.

[2] M. Kokkinakis, I. Tsakiris, M. Tzatzarakis, E. Vakonaki, A. Alegakis, S. Papachristou, V. Karzi, A. Kokkinaki, M. Goumenou, M. Kallionakis, A. Kalogeraki, Carcinogenic, ethanol, acetaldehyde and noncarcinogenic higher alcohols, esters, and methanol compounds found in traditional alcoholic beverages. A risk assessment approach, Toxicol. Rep. 7 (2020) 1057–1065. https://doi.org/10.1016/j.toxrep.2020.08.017.

[3] M. Peplow, Alcohol fuels not so green, Nature. (2005). https://doi.org/10.1038/news050627-15.

[4] F.E. Ahmed, Toxicological effects of ethanol on human health, Crit. Rev. Toxicol. 25 (1995) 347–367. https://doi.org/10.3109/10408449509021614.

[5] W.J. Criddle, ETHANOL, in: P. Worsfold, A. Townshend, C. Poole (Eds.), Encycl. Anal. Sci. Second Ed., Elsevier, Oxford, 2005: pp. 562–569. https://doi.org/10.1016/B0-12-369397-7/00148-5.

[6] B. Strohm, Ethanol, in: P. Wexler (Ed.), Encycl. Toxicol. Third Ed., Academic Press, Oxford, 2014: pp. 488–491. https://doi.org/10.1016/B978-0-12-386454-3.00379-1.

[7] M.M. Rahman, M.M. Alam, A.M. Asiri, M.A. Islam, Ethanol sensor development based on ternary-doped metal oxides ($CdO/ZnO/Yb_2O_3$) nanosheets for environmental safety, RSC Adv. 7 (2017) 22627–22639. https://doi.org/10.1039/C7RA01852E.

[8] S. Reiß, G. Hagen, R. Moos, Zeolite-based Impedimetric Gas Sensor Device in Low-cost Technology for Hydrocarbon Gas Detection, Sensors. 8 (2008) 7904–7916. https://doi.org/10.3390/s8127904.

[9] J. van den Broek, I.C. Weber, A.T. Güntner, S.E. Pratsinis, Highly selective gas sensing enabled by filters, Mater. Horiz. 8 (2021) 661–684. https://doi.org/10.1039/D0MH01453B.

[10] W.L. Rauch, M. Liu, Development of a selective gas sensor utilizing a perm-selective zeolite membrane, J. Mater. Sci. 38 (2003) 4307–4317. https://doi.org/10.1023/A:1026331015093.

[11] N.V. Choudary, B.L. Newalkar, Use of zeolites in petroleum refining and petrochemical processes: recent advances, J. Porous Mater. 18 (2011) 685–692. https://doi.org/10.1007/s10934-010-9427-8.

[12] T.W. Wong, Handbook of Zeolites: Structure, Properties and Applications, Nova Science Publishers, 2009.

[13] C.J. Rhodes, Properties and applications of Zeolites, Sci. Prog. 93 (2010) 223–284. https://doi.org/10.3184/003685010X12800828155007.

[14] H. Gies, Pore show, Nature. 437 (2005) 633–633. https://doi.org/10.1038/437633a.

[15] E. Grifoni, G. Piccini, J.A. Lercher, V.-A. Glezakou, R. Rousseau, M. Parrinello, Confinement effects and acid strength in zeolites, Nat. Commun. 12 (2021) 2630. https://doi.org/10.1038/s41467-021-22936-0.

[16] A.L. Janda, Effects of Zeolite Structure and Si/Al Ratio on Adsorption Thermodynamics and Intrinsic Kinetics of Monomolecular Cracking and Dehydrogenation of Alkanes over Brønsted Acid Sites, 192.

[17] J.M. Newsam, The Zeolite Cage Structure, Science. 231 (1986) 1093–1099. https://doi.org/10.1126/science.231.4742.1093.

[18] L.-H. Chen, M.-H. Sun, Z. Wang, W. Yang, Z. Xie, B.-L. Su, Hierarchically Structured Zeolites: From Design to Application, Chem. Rev. 120 (2020) 11194–11294. https://doi.org/10.1021/acs.chemrev.0c00016.
[19] Database of Zeolite Structures, http://www.iza-structure.org/databases.
[20] S. Li, W.F. Schneider, Supercell Models of Brønsted and Lewis Sites in Zeolites, in: W. Andreoni, S. Yip (Eds.), Handb. Mater. Model. Appl. Curr. Emerg. Mater., Springer International Publishing, Cham, 2018: pp. 1–21. https://doi.org/10.1007/978-3-319-50257-1_4-1.
[21] M. Ravi, V.L. Sushkevich, J.A. van Bokhoven, Towards a better understanding of Lewis acidic aluminium in zeolites, Nat. Mater. 19 (2020) 1047–1056. https://doi.org/10.1038/s41563-020-0751-3.
[22] A. Palčić, V. Valtchev, Analysis and control of acid sites in zeolites, Appl. Catal. Gen. 606 (2020) 117795. https://doi.org/10.1016/j.apcata.2020.117795.
[23] G. Li, E.A. Pidko, The Nature and Catalytic Function of Cation Sites in Zeolites: a Computational Perspective, ChemCatChem. 11 (2019) 134–156. https://doi.org/10.1002/cctc.201801493.
[24] B. Orazbayev, D. Kozhakhmetova, R. Wójtowicz, J. Krawczyk, Modeling of a Catalytic Cracking in the Gasoline Production Installation with a Fuzzy Environment, Energies. 13 (2020) 4736. https://doi.org/10.3390/en13184736.
[25] X. Xu, J. Wang, Y. Long, Zeolite-based Materials for Gas Sensors, Sensors. 6 (2006) 1751–1764. https://doi.org/10.3390/s6121751.
[26] Y. Zheng, X. Li, P.K. Dutta, Exploitation of Unique Properties of Zeolites in the Development of Gas Sensors, Sensors. 12 (2012) 5170–5194. https://doi.org/10.3390/s120405170.
[27] X. Li, S. Song, Q. Shuai, Y. Pei, T. Aastrup, Y. Pei, Z. Pei, Real-time and label-free analysis of binding thermodynamics of carbohydrate-protein interactions on unfixed cancer cell surfaces using a QCM biosensor, Sci. Rep. 5 (2015) 14066. https://doi.org/10.1038/srep14066.
[28] B. Becker, M.A. Cooper, A survey of the 2006-2009 quartz crystal microbalance biosensor literature, J. Mol. Recognit. 24 (2011) 754–787. https://doi.org/10.1002/jmr.1117.
[29] S. Lakkis, R. Younes, Y. Alayli, M. Sawan, Review of recent trends in gas sensing technologies and their miniaturization potential, Sens. Rev. 34 (2014) 24–35. https://doi.org/10.1108/SR-11-2012-724.
[30] M.D. Ward, D.A. Buttry, In Situ Interfacial Mass Detection with Piezoelectric Transducers, Science. 249 (1990) 1000–1007. https://doi.org/10.1126/science.249.4972.1000.
[31] O. Delgado-Friedrichs, M.D. Foster, M. O'Keeffe, M.M.J. Treacy, Potential Zeolites Related to Faujasite: Structures and Energetics, Cryst. Growth Des. 20 (2020) 6896–6902. https://doi.org/10.1021/acs.cgd.0c00946.
[32] S. Hashimoto, Zeolite photochemistry: impact of zeolites on photochemistry and feedback from photochemistry to zeolite science, J. Photochem. Photobiol. C Photochem. Rev. 4 (2003) 19–49. https://doi.org/10.1016/S1389-5567(03)00003-0.
[33] J. Rouquerol, F. Rouquerol, P. Llewellyn, G. Maurin, K.S.W. Sing, Adsorption by Powders and Porous Solids: Principles, Methodology and Applications, Academic Press, 2013.
[34] L. Zoubida, B. Hichem, The Nanostructure Zeolites MFI-Type ZSM5, in: C.M. Simonescu (Ed.), Nanocrystals Nanostructures, InTech, 2018. https://doi.org/10.5772/intechopen.77020.

[35] N. Cui, H. Guo, J. Zhou, L. Li, L. Guo, Z. Hua, Regulation of framework Al distribution of high-silica hierarchically structured ZSM-5 zeolites by boron-modification and its effect on materials catalytic performance in methanol-to-propylene reaction, Microporous Mesoporous Mater. 306 (2020) 110411. https://doi.org/10.1016/j.micromeso.2020.110411.
[36] F. Daeyaert, M.W. Deem, Design of organic structure directing agents for polymorph A zeolite beta, J. Mater. Chem. A. 7 (2019) 9854–9866. https://doi.org/10.1039/C8TA11913A.
[37] J.B. Higgins, R.B. LaPierre, J.L. Schlenker, A.C. Rohrman, J.D. Wood, G.T. Kerr, W.J. Rohrbaugh, The framework topology of zeolite beta, Zeolites. 8 (1988) 446–452. https://doi.org/10.1016/S0144-2449(88)80219-7.
[38] M.D. González, Y. Cesteros, P. Salagre, Comparison of dealumination of zeolites beta, mordenite and ZSM-5 by treatment with acid under microwave irradiation, Microporous Mesoporous Mater. 144 (2011) 162–170. https://doi.org/10.1016/j.micromeso.2011.04.009.
[39] P.S. Bárcia, J.A.C. Silva, A.E. Rodrigues, Adsorption equilibrium and kinetics of branched hexane isomers in pellets of BETA zeolite, Microporous Mesoporous Mater. 79 (2005) 145–163. https://doi.org/10.1016/j.micromeso.2004.10.037.
[40] N.D. Shcherban, R.Yu. Barakov, P. Mäki-Arvela, S.A. Sergiienko, I. Bezverkhyy, K. Eränen, D.Yu. Murzin, Isomerization of α-pinene oxide over ZSM-5 based micro-mesoporous materials, Appl. Catal. Gen. 560 (2018) 236–247. https://doi.org/10.1016/j.apcata.2018.05.007.
[41] G. Laugel, X. Nitsch, F. Ocampo, B. Louis, Methanol dehydration into dimethylether over ZSM-5 type zeolites: Raise in the operational temperature range, Appl. Catal. Gen. 402 (2011) 139–145. https://doi.org/10.1016/j.apcata.2011.05.039.
[42] R. Barakov, N. Shcherban, P. Yaremov, I. Bezverkhyy, J. Čejka, M. Opanasenko, Hierarchical Beta zeolites as catalysts in a one-pot three-component cascade Prins–Friedel–Crafts reaction, Green Chem. 22 (2020) 6992–7002. https://doi.org/10.1039/D0GC01787F.
[43] Y. Li, H. Wang, M. Dong, J. Li, Z. Qin, J. Wang, W. Fan, Effect of zeolite pore structure on the diffusion and catalytic behaviors in the transalkylation of toluene with 1,2,4-trimethylbenzene, RSC Adv. 5 (2015) 66301–66310. https://doi.org/10.1039/C5RA09236A.
[44] M. Giraudet, I. Bezverkhyy, G. Weber, C. Dirand, M. Macaud, J.-P. Bellat, D2/H2 adsorption selectivity on FAU zeolites at 77.4 K: Influence of Si/Al ratio and cationic composition, Microporous Mesoporous Mater. 270 (2018) 211–219. https://doi.org/10.1016/j.micromeso.2018.05.026.
[45] M. Ravi, V. L. Sushkevich, J.A. van Bokhoven, On the location of Lewis acidic aluminum in zeolite mordenite and the role of framework-associated aluminum in mediating the switch between Brønsted and Lewis acidity, Chem. Sci. 12 (2021) 4094–4103. https://doi.org/10.1039/D0SC06130A.
[46] C.-C. Chang, H.J. Cho, Z. Wang, X. Wang, W. Fan, Fluoride-free synthesis of a Sn-BEA catalyst by dry gel conversion, Green Chem. 17 (2015) 2943–2951. https://doi.org/10.1039/C4GC02457E.
[47] H. Chiang, A. Bhan, Catalytic consequences of hydroxyl group location on the rate and mechanism of parallel dehydration reactions of ethanol over acidic zeolites, J. Catal. 271 (2010) 251–261. https://doi.org/10.1016/j.jcat.2010.01.021.
[48] K. Gołąbek, E. Tabor, V. Pashkova, J. Dedecek, K. Tarach, K. Góra-Marek, The proximity of aluminium atoms influences the reaction pathway of ethanol transformation

over zeolite ZSM-5, Commun. Chem. 3 (2020) 1–9. https://doi.org/10.1038/s42004-020-0268-3.
[49] C.-C. Lee, R.J. Gorte, W.E. Farneth, Calorimetric Study of Alcohol and Nitrile Adsorption Complexes in H-ZSM-5, J. Phys. Chem. B. 101 (1997) 3811–3817. https://doi.org/10.1021/jp970711s.
[50] M.-M. Yang, X.-H. Bao, W.-X. Li, First Principle Study of Ethanol Adsorption and Formation of Hydrogen Bond on Rh(111) Surface, J. Phys. Chem. C. 111 (2007) 7403–7410. https://doi.org/10.1021/jp0686184.
[51] S. Caro-Ortiz, E. Zuidema, M. Rigutto, D. Dubbeldam, T.J.H. Vlugt, Effects of Framework Flexibility on the Adsorption and Diffusion of Aromatics in MFI-Type Zeolites, J. Phys. Chem. C. 124 (2020) 24488–24499. https://doi.org/10.1021/acs.jpcc.0c08054.
[52] J.A. Laksmono, U.A. Pangesti, M. Sudibandriyo, A. Haryono, A.H. Saputra, Adsorption capacity study of ethanol-water mixture for zeolite, activated carbon, and polyvinyl alcohol, IOP Conf. Ser. Earth Environ. Sci. 105 (2018) 012025. https://doi.org/10.1088/1755-1315/105/1/012025.
[53] J. S. Bates, B. C. Bukowski, J. Greeley, R. Gounder, Structure and solvation of confined water and water–ethanol clusters within microporous Brønsted acids and their effects on ethanol dehydration catalysis, Chem. Sci. 11 (2020) 7102–7122. https://doi.org/10.1039/D0SC02589E.
[54] E. Haghighi, S. Zeinali, Formaldehyde detection using quartz crystal microbalance (QCM) nanosensor coated by nanoporous MIL-101(Cr) film, Microporous Mesoporous Mater. 300 (2020) 110065. https://doi.org/10.1016/j.micromeso.2020.110065.
[55] N. Pfriem, P.H. Hintermeier, S. Eckstein, S. Kim, Q. Liu, H. Shi, L. Milakovic, Y. Liu, G.L. Haller, E. Baráth, Y. Liu, J.A. Lercher, Role of the ionic environment in enhancing the activity of reacting molecules in zeolite pores, Science. (2021). https://doi.org/10.1126/science.abh3418.
[56] Y. Li, H. Wang, M. Dong, J. Li, Z. Qin, J. Wang, W. Fan, Effect of zeolite pore structure on the diffusion and catalytic behaviors in the transalkylation of toluene with 1,2,4-trimethylbenzene, RSC Adv. 5 (2015) 66301–66310. https://doi.org/10.1039/C5RA09236A.
[57] C.H.L. Tempelman, R. Oozeerally, V. Degirmenci, Heterogeneous Catalysts for the Conversion of Glucose into 5-Hydroxymethyl Furfural, Catalysts. 11 (2021) 861. https://doi.org/10.3390/catal11070861.
[58] O. Zybaylo, O. Shekhah, H. Wang, M. Tafipolsky, R. Schmid, D. Johannsmann, C. Wöll, A novel method to measure diffusion coefficients in porous metal–organic frameworks, Phys. Chem. Chem. Phys. 12 (2010) 8093–8098. https://doi.org/10.1039/B927601G.
[59] P.M. Veiga, A.C.L. Gomes, C.O. Veloso, C.A. Henriques, Acid zeolites for glycerol etherification with ethyl alcohol: Catalytic activity and catalyst properties, Appl. Catal. Gen. 548 (2017) 2–15. https://doi.org/10.1016/j.apcata.2017.06.042.
[60] N.S. Gould, S. Li, H.J. Cho, H. Landfield, S. Caratzoulas, D. Vlachos, P. Bai, B. Xu, Understanding solvent effects on adsorption and protonation in porous catalysts, Nat. Commun. 11 (2020) 1060. https://doi.org/10.1038/s41467-020-14860-6.
[61] Ł. Kuterasiński, U. Filek, M. Gackowski, M. Zimowska, M. Ruggiero-Mikołajczyk, P.J. Jodłowski, Sonochemically prepared hierarchical MFI-type zeolites as active catalysts for catalytic ethanol dehydration, Ultrason. Sonochem. 74 (2021) 105581. https://doi.org/10.1016/j.ultsonch.2021.105581.
[62] I.N. Senchenya, V.B. Kazansky, Quantum chemical studies of ethylene interaction with zeolite OH-groups, Catal. Lett. 8 (1991) 317–325. https://doi.org/10.1007/BF00764193.

[63] J.N. Kondo, D. Nishioka, H. Yamazaki, J. Kubota, K. Domen, T. Tatsumi, Activation Energies for the Reaction of Ethoxy Species to Ethene over Zeolites, J. Phys. Chem. C. 114 (2010) 20107–20113. https://doi.org/10.1021/jp107082t.
[64] Y. Chen, X. Li, X. Li, J. Wang, Z. Tang, UV activated hollow ZnO microspheres for selective ethanol sensors at low temperatures, Sens. Actuators B Chem. 232 (2016) 158–164. https://doi.org/10.1016/j.snb.2016.03.138.
[65] D. Sebők, L. Janovák, D. Kovács, A. Sápi, D.G. Dobó, Á. Kukovecz, Z. Kónya, I. Dékány, Room temperature ethanol sensor with sub-ppm detection limit: Improving the optical response by using mesoporous silica foam, Sens. Actuators B Chem. 243 (2017) 1205–1213. https://doi.org/10.1016/j.snb.2016.12.097.
[66] X.J. Li, S.J. Chen, C.Y. Feng, Characterization of silicon nanoporous pillar array as room-temperature capacitive ethanol gas sensor, Sens. Actuators B Chem. 123 (2007) 461–465. https://doi.org/10.1016/j.snb.2006.09.021.
[67] T. Takahashi, Y.-J. Choi, K. Sawada, K. Takahashi, A ppm Ethanol Sensor Based on Fabry–Perot Interferometric Surface Stress Transducer at Room Temperature, Sensors. 20 (2020) 6868. https://doi.org/10.3390/s20236868.
[68] S. Zhan, D. Li, S. Liang, X. Chen, X. Li, A Novel Flexible Room Temperature Ethanol Gas Sensor Based on SnO2 Doped Poly-Diallyldimethylammonium Chloride, Sensors. 13 (2013) 4378–4389. https://doi.org/10.3390/s130404378.
[69] A. Bello, F. Bianchi, M. Careri, M. Giannetto, V. Mastria, G. Mori, M. Musci, Potentialities of a modified QCM sensor for the detection of analytes interacting via H-bonding and application to the determination of ethanol in bread, Sens. Actuators B Chem. 125 (2007) 321–325. https://doi.org/10.1016/j.snb.2007.02.021.

Table 1

Channel system and textural properties (A_{BET}: BET area, V_T: Total pore volume and D_m: average pore diameter) of DaY, ZSM-5 and BEA [40,42–44].

Adsorbent	Channel system				Textural properties		
	Dimension	Windows	Channel diameter (Å)	Channel intersection dimension (Å)	A_{BET} (m^2/g)	V_T (cm^3/g)	D_m (Å)
DaY	3	12-MR	7.4 × 7.4	12 × 12 × 12	716	0.31	11.2
ZSM-5	3	10-MR	5.4 × 5.6 5.1 × 5.5	8.6	393	0.18	5.5
BEA	3	12-MR	6.6 × 6.7 5.6 × 5.7	13.9	529	0.22	7.5

Table 2

Comparison between this work and reported previous methods on sensor response, response time, and recovery time at room temperature for ethanol detection.

Ethanol detection methods	Concentration	Sensor response	Response time (t_{Rs})	Response time (t_{Rv})	Ref.
UV activated ZnO: MEMS	10 ppm	10 %[a]	80 s	-	[64]
ZnO_2/PAA[*]/ZnO_2/SF[#]: optical sensor	12 ppm	~ 8 nm[b]	40 s	80 s	[65]
Silicon nanoporous pillar array: Capitance	50 ppm	7 %[c]	15 s	30 s	[66]
PMMA[**]/parylene-C membrane: Surface sensor	5 ppm	500 µN/m[d]	-	-	[67]
SnO_2 doped PDDAC[##] : flexible sensor	10 ppm	17 %[a]	> 5 min	> 8 min	[68]
Polyaniline coated QCM	3ppm	12×10^{-4} [e]	> 3 min	> 1 min	[69]
BEA coated QCM	10 ppm	8.8×10^{-6} [e]	36 s	18 s	Present work

Poly(acrylic acid)[*], Silica foam[#], polymethyl methacrylate**, Poly Diallyldimethylammonium Chloride[##]; Sensor response, $R_{res}(\%)^a = (I_m-I_s)/I_m \times 100$, $R_{res}{}^b = \lambda_{air} - \lambda_{ethanol}$, $R_{res}(\%)^c = \Delta C/C \times 100$, $R_{res}{}^d = \sigma_{air} - \sigma_{air}$, $R_{res}{}^e = \Delta f / f_0$.

Figure Caption

Fig. 1 Schematic of Brønsted and Lewis acid sites in zeolite [24].

Fig. 2 (a) Photographs of pristine quartz specs (~13.9 mm diameter) with Au/Ti electrodes in the middle and with a coated adsorbent (BEA) with a diameter of ~5.0 mm, (b) N_2 Adsorption – desorption isotherms for DaY, ZSM-5, and BEA, and (c) SEM images of DaY, ZSM-5 and BEA.

Fig. 3 FTIR spectra of DaY, ZSM-5 and BEA. Orange, grey and blue represent the bands position of Lewis acid (LA) sites, Brønsted acid (BA) sites and OH stretching [45,46], respectively.

Fig. 4 Steps of ethanol chemisorption on zeolite's surface (a) Bonded ethanol monomer, (b) dimeric ethanol species, and (c) ethoxy group [47–49].

Fig. 5 Relative frequency reversible curves as the function of time for ethanol sensing at 10, 20, and 30 ppm of (a) DaY, (c) ZSM-5, and (e) BEA coated QCM sensor, and the response and recovery times for (b) DaY, (d) ZSM-5, and (f) BEA with varying ethanol concentrations. The error-bars represent the standard deviation over five trials.

Fig. 6 Plot of $\frac{f_t}{f_\infty}$ vs. $t^{1/2}$ with the initial point linear fitting (in red) of: (a) DaY, (b) ZSM-5 and (c) BEA coated QCM sensor.

Fig. 7 Proposed ethanol sensing mechanism for zeolite coated QCM sensor, steps (i) to (iv) are devoted for the adsorption process, and steps (v) to (vii) are devoted for the desorption process.

Fig. 1

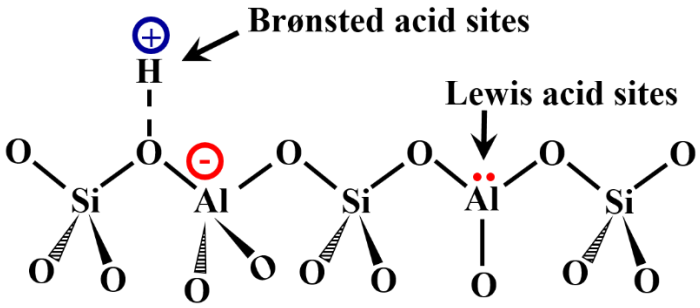

Fig. 2

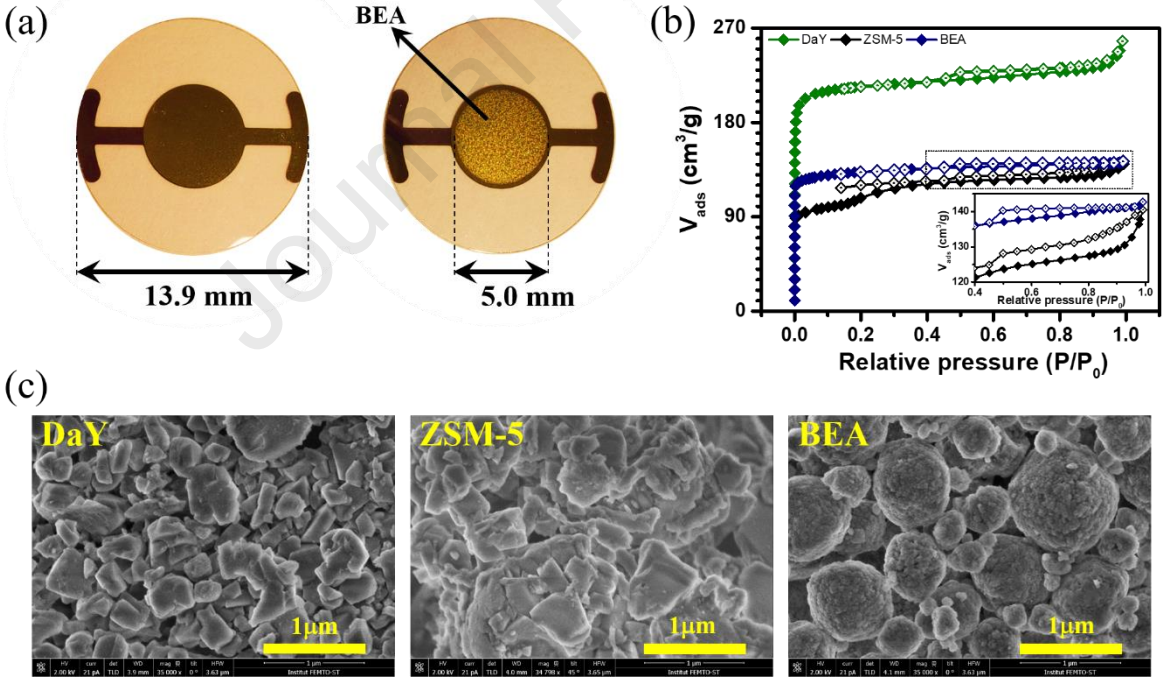

Fig. 3

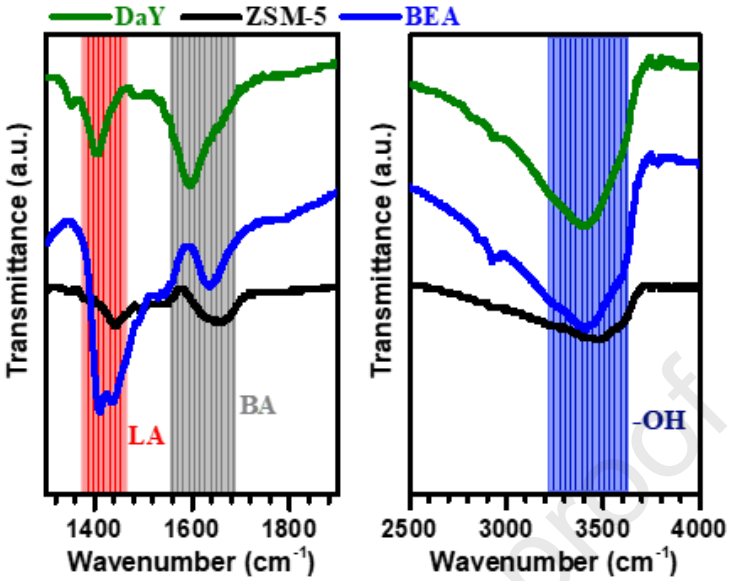

Fig. 4

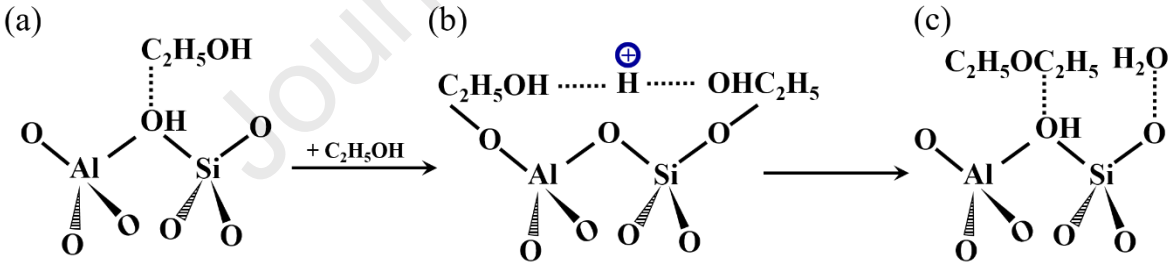

Fig. 5

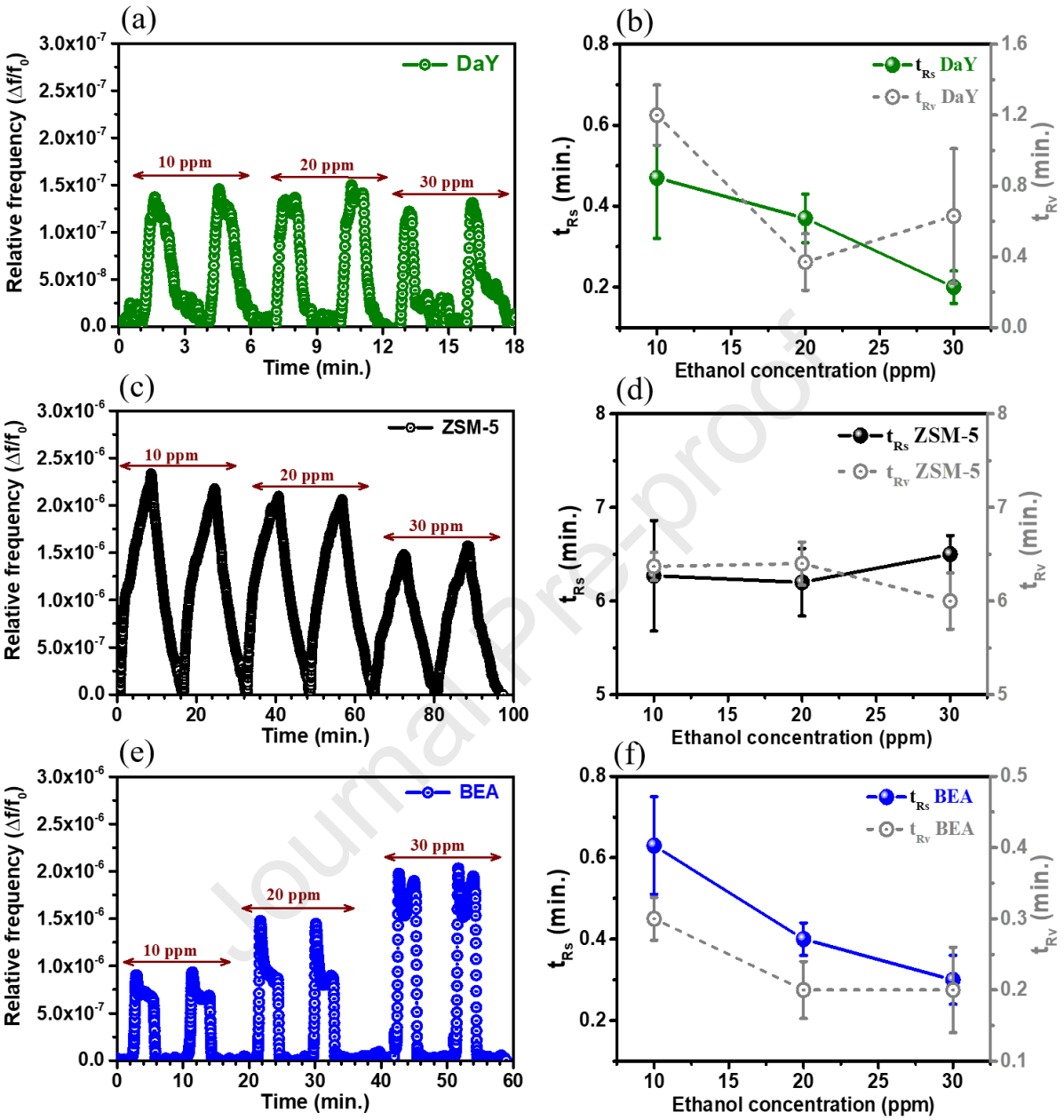

Fig. 6

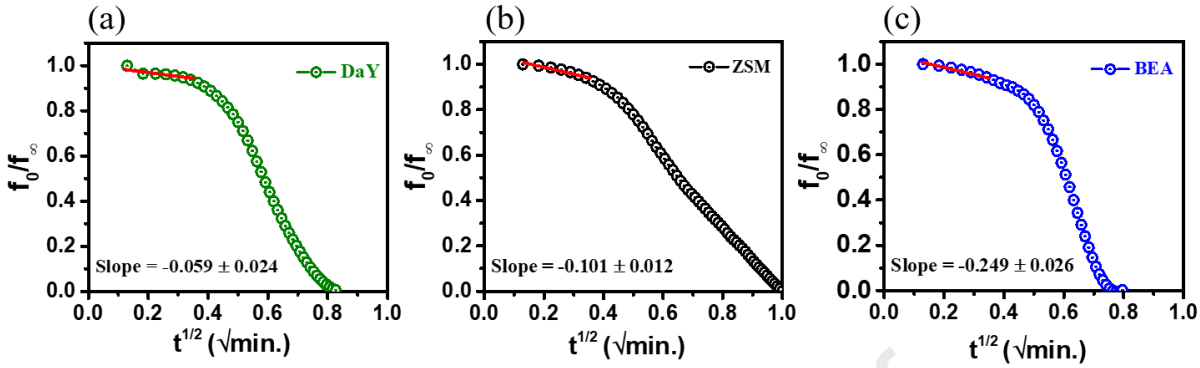

Fig. 7

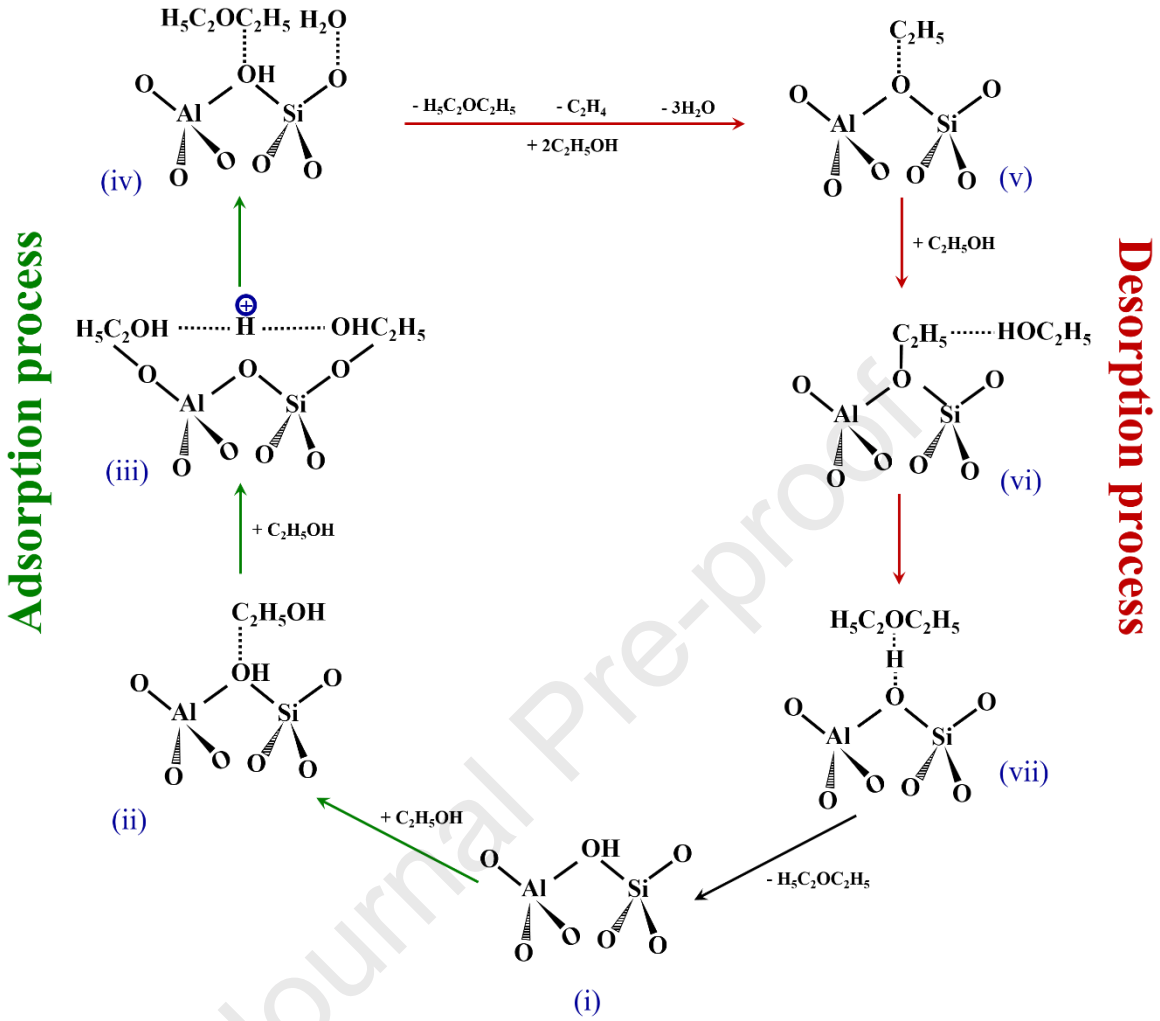

Highlights

- Zeolite coated QCM was used for ethanol sensing at room temperature.
- Lewis acid sites density and the micro-mesoporous connectivity are the key parameters for ethanol sensing.
- BEA coated QCM exhibited excellent sensing performances for ethanol at room temperature.
- The sensing mechanism of ethanol with the BEA zeolite is presented and thoroughly explained.

Declaration of interests

☒ The authors declare that they have no known competing financial interests or personal relationships that could have appeared to influence the work reported in this paper.

☐The authors declare the following financial interests/personal relationships which may be considered as potential competing interests: